# Nonlinear dynamics of a spin-orbit-coupled Bose-Einstein condensate

Yongping Zhang,* Zhiqian Gui, and Yuanyuan Chen

*Department of Physics, Shanghai University, Shanghai 200444, China*

Single-particle dynamics of a spin-orbit-coupled Bose-Einstein condensate has recently been investigated in experiments that explore the physics of Landau-Zener tunneling and of the Zitterbewegung. In this paper, we study the influence of a nonlinearity due to interactions on these dynamics and show that the dispersion relation develops interesting loop strucures. The atoms can move along the nonlinear dispersion curve in the presence of a weak acceleration force and we show that the loops lead to straightforward nonlinear Landau-Zener tunneling. However, we find that for the Zitterbewegung, induced by a sudden quench in the spin-orbit coupling parameters, the nonlinear dispersion is irrelevant.

Since the experimental implementation of artificial spin-orbit coupling in atomic Bose-Einstein condensates (BECs) [1], a great deal of attention has been paid to the physics of spin-orbit-coupled neutral atoms (see, e.g., [2–8] and reference therein). For a two-component BEC, experimentally realizable one-dimensional spin-orbit coupling [1, 9] gives rise to an energy-quasimomentum dispersion relation featuring two energy bands with a double well structure in lower branch. This novel dispersion behaviour greatly enriches the ground-state phase diagram [10–17] and the collective excitation dynamics [18–21], compared with the parabolic dispersion of ordinary atomic BECs. By control over experimental parameters, dynamics involving two spin-orbit-coupled bands can be excited and it has been shown experimentally that a quantum quench can result in intriguing Zitterbewegung oscillations [22]. Experimental confirmation also exists for identifying the transitions between two bands due to an acceleration as being of Landau-Zener type [23]. Both of these two experiments deal with manybody systems, in which the nonlinearity stemming from the atomic interactions cannot be neglected. Nevertheless, the experimental measurements can be completely explained by utilizing single-particle spin-orbit-coupled bands [22, 23] and the role of nonlinearity in these dynamics remains to be explored. Very recently, the experimental group at MIT has pushed spin-orbit-coupled BECs into a new regime where the nonlinear coefficients are fully tunable [24].

In this work, we theoretically study the dynamics of a spin-orbit-coupled BEC and explicitly consider the nonlinear effects. Similarly to the experiments in Refs. [22, 23], we study two different approaches to trigger nonlinear dynamics, one is by a weak acceleration force and the other is by a quench. We intuitively expect that the nonlinear dynamics follows the nonlinear energy-quasimomentum dispersion based on single-particle physics. However, our results demonstrate that depending on the way the dynamics is initiated, the system responds distinctly different to the nonlinear dispersion. When the acceleration force is weak compared to the energy difference between the two spin-orbit-coupled bands, it drives the atoms to adiabatically move along the nonlinear spin-orbit-coupled bands. In addition, for certain nonlinear coefficients regimes, a loop-like structure appears in the nonlinear dispersion relation. This is an entirely nonlinear effect without a linear analog. The loops break the adiabatic motion of the atoms, even while the acceleration force is weak, leading to nonlinear Landau-Zener transitions [25–27] between two nonlinear spin-orbit-coupled bands. We propose to measure the sizes of the loop structures by taking advantage of nonlinear Landau-Zener transitions. We show that for the acceleration force induced dynamics the nonlinear dispersion relation is fully relevant. We next study quench dynamics induced by a sudden jump of the spin-orbit coupling parameters and show that the resulting dynamics has no connection to the nonlinear dispersion. The resulted dynamics shows periodic oscillation, whose frequency does not match with energy difference between the two nonlinear bands, which is distinctly different from the single-particle dynamics, where atoms oscillate between single-particle bands. In fact, the presence of a nonlinearity breaks the quantum superposition principle, such that nonlinear bands can not form a complete basis to support dynamics. Despite the presence of the nonlinearity in the system, the quench dynamics experiments in [22] follow single-particle bands, and we show that the experiments can therefore be effectively interpreted as single-particle systems.

The dynamics of a spin-orbit-coupled Bose-Einstein condensate obeys the dimensionless Gross-Pitaevskii (GP) equation,

$$i\frac{\partial \Psi}{\partial t} = (H_{\text{soc}} + H_{\text{non}}[\Psi])\Psi, \tag{1}$$

where the wave function is a spinor $\Psi = [\Psi_1, \Psi_2]^T$. $H_{\text{soc}}$ is the single-particle spin-orbit-coupled Hamiltonian,

$$H_{\text{soc}} = -\frac{1}{2}\frac{\partial^2}{\partial x^2} - i\gamma\frac{\partial}{\partial x}\sigma_z + \frac{\delta}{2}\sigma_z + \frac{\Omega}{2}\sigma_x, \tag{2}$$
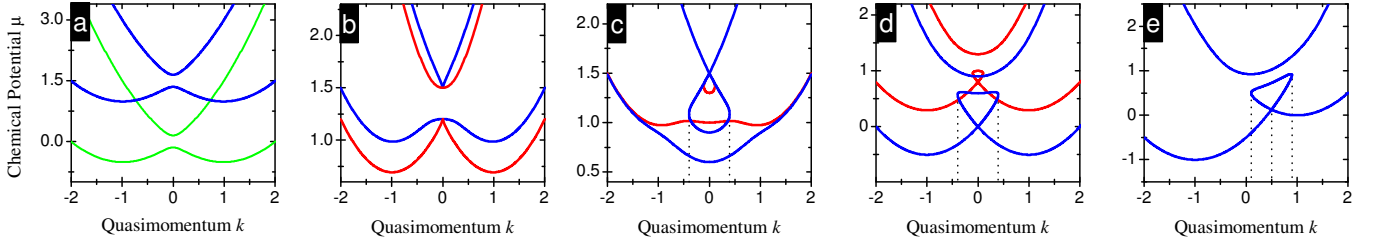
FIG. 1. Nonlinear dispersion relation $\mu(k)$ for $g_{11} = g_{22} = g$, $\Omega = 0.3$ and $\gamma = 1$. (a): Comparison of the nonlinear dispersion with equal nonlinear coefficients $g_{12} = g = 1.5$ (blue lines) with the linear dispersion $g_{12} = g = 0$ (green lines). (b): Cusps can be seen to develop in the upper branch (blue lines) for $g = 1.5, g_{12} = 1.2$ and in the lower branch (red lines) for $g = 1.2, g_{12} = 1.5$. (c): Loops appear in the upper branch and their sizes change with different nonlinear coefficients. Red lines are for $g = 1.5$ and $g_{12} = 0.8$, and blue lines are for $g = 1.5$ and $g_{12} = 0$. (d): Loops exist in the lower branch, red lines are for $g = 0.8$ and $g_{12} = 1.5$ and blue lines are for $g = 0$ and $g_{12} = 1.5$. In (a)-(d), $\delta = 0$. (e): Loop structure with a finite detuning $\delta = -1$ for $g = 0$ and $g_{12} = 1.5$. The vertical dashed lines in (c)-(e) label the locations of the edges and the center of the loop structures.

and $H_{\text{non}}$ accounts for the interactions,

$$H_{\text{non}}[\Psi] = \begin{pmatrix} g_{11}|\Psi_1|^2 + g_{12}|\Psi_2|^2 & 0 \\ 0 & g_{12}|\Psi_1|^2 + g_{22}|\Psi_2|^2 \end{pmatrix}. \quad (3)$$

The one dimensional spin-orbit coupling is generated experimentally by applying two Raman beams that couple two pseudo-spin states [1, 9, 17, 18, 20–24]. $\gamma$ characterizes the spin-orbit coupling strength $\hbar k_{\text{Ram}}/m$ with $k_{\text{Ram}}$ being wave number of Raman beams, $\delta$ is the detuning, and $\Omega$ is the Rabi frequency. In the dimensionless GP equation, the units of energy, length and time are $\hbar^2 k_{\text{Ram}}^2/m$ , $1/k_{\text{Ram}}$ and $m/(\hbar k_{\text{Ram}}^2)$, respectively. Such scales lead to $\gamma = 1$, however it can be varied to be $\gamma \leq 1$ by performing a high-frequency driving of the intensity of the Raman lasers [28, 29]. We therefore only consider $0 < \gamma \leq 1$, since the physics in the $\gamma < 0$ regime is same as that in the regime of $\gamma > 0$. This is because the GP equation possesses a spin rotation symmetry, i.e., $U = \sigma_x$, when also flipping the signs of $\gamma$ and $\delta$. The nonlinear coefficients $g_{ij}$ are proportional to the s-wave scattering lengths and atom numbers, and can be adjusted in experiments [24].

Guided by the fact that single-particle dynamics follows from the single-particle energy dispersion relation, we first analyse the nonlinear dispersion relation of our system in order to understand the nonlinear dynamics. This can be done by assuming that the solution of Eq. (1) is a plane wave function, i.e., $\Psi = \exp(ikx - i\mu t)\Phi$, with $k$ being quasimomentum in units of $k_{Ram}$, and $\mu$ being the chemical potential. $\Phi = [\Phi_1, \Phi_2]^T$ then admits a time-independent GP equation,

$$\mu\Phi = (H_{\text{soc}}(k)\Phi + H_{\text{non}}[\Phi]) \Phi, \quad (4)$$

where the single-particle Hamiltonian in momentum space can be written as, $H_{\text{soc}}(k) = k^2/2 + \gamma k\sigma_z + \delta\sigma_z/2 + \Omega\sigma_x/2$. Meanwhile, $\Phi$ satisfies the renormalization condition $|\Phi_1|^2 + |\Phi_2|^2 = 1$.

The nonlinear dispersion relation $\mu(k)$, i.e., chemical potential as a function of the quasimomentum $k$, can be numerically calculated from Eq. (4) for different values of the nonlinear coefficients. For simplicity, in the following, we consider $g_{11} = g_{22} = g$ and show typical results in Fig. 1. Since we consider two atomic components, the dispersion relation possesses two branches. If all nonlinear coefficients are equal, i.e. $g_{12} = g$, we find that the nonlinear dispersion is just an overall upward displacement of its linear counterpart [see Fig. 1(a)]. If the inter-species interaction is not equal to the intra-species interactions, i.e. $g_{12} \neq g$, the nonlinear dispersion relation develops several interesting features: (1) at certain values of the nonlinear coefficients a cusp appears in upper or lower band [see Fig. 1(b)]; (2) loop structures can arise in the upper or lower branch [see Figs. 1(c) and 1(d)]. The sizes of the loops depend on the nonlinear coefficients; (3) moreover, the detuning can tilt the loops and shift their location in momentum space, as shown in Fig. 1(e).

Spin-orbit-coupled BECs are not the only systems to support the existence of loop structures in the nonlinear dispersion relation. They have been investigated theoretically and experimentally in various nonlinear systems, ranging from BECs in optical lattices [30–37], in optical cavities [38, 39], in Bragg gratings [40], with Dirac cones [41, 42], and exciton-polariton condensates [43] to degenerate Fermi gases [44, 45]. A typical and simple system to study loop-features in nonlinear dispersion relations is a two-level avoided crossing [25, 26]. When nonlinear effects overcome the gap size of the avoided crossing, some nonlinear solutions without linear analogues emerge and, interestingly, they can form a closed loops in the dispersion relation.

In order to understand the underlying physics of the general results depicted in Fig. 1, we therefore map our system onto a standard nonlinear two-level model [25, 26]. By using the renormalization condition $|\Phi_1|^2 + |\Phi_2|^2 = 1$, we re-write Eq. (4) as, $\mu_{\text{ntl}}\Phi = H_{\text{ntl}}\Phi$,

with $\mu_{\rm ntl} = \mu - (g + g_{12})/2 - k^2/2$, and the nonlinear two-level Hamiltonian $H_{\rm ntl}$ is,

$$H_{\rm ntl} = \left(\gamma k + \frac{\delta}{2}\right)\sigma_z + \frac{g_{12}-g}{2}\left(|\Phi_2|^2 - |\Phi_1|^2\right)\sigma_z + \frac{\Omega}{2}\sigma_x,$$
(5)

where the $\sigma$ are the Pauli matrices. The linear parts (the first and third term) defines an avoided crossing in momentum space, and an energy gap is opened of size $\Omega$ at $k = -\delta/(2\gamma)$. The competition between the nonlinear (second term) and the linear parts is mainly represented by the non-commutation between the nonlinear term $(g_{12}-g)(|\Phi_2|^2 - |\Phi_1|^2)\sigma_z/2$ and the gap size term $\Omega\sigma_x/2$. When the nonlinear term dominates over the gap size, $|g_{12}-g| > \Omega$, loop structures appear [25, 26]. The critical condition $|g_{12}-g| = \Omega$ is special, as at this point a cusp [see Fig. 1(b)] develops to prepare the dispersion relation for the emerging loop structures. When $g_{12} - g > \Omega$, new nonlinear solutions without linear analogues bifurcate from the lower branch and extend upwards into energy gap since the effective nonlinearity is repulsive if $g_{12} - g > 0$. These new solutions form a loop attached to the lower dispersion branch as seen in Fig. 1(d). If $g_{12} - g < 0$, the effective nonlinearity is attractive, and when $g_{12} - g < -\Omega$, the loop structure bifurcates from the upper branch [see Fig. 1(c)].

The center of the loops locates at $k = -\delta/(2\gamma)$, where the gap in the linear dispersion relation has a minimum. Therefore, the finite value of $\delta$ can displace the location of loops, as can be seen in Fig. 1(e). Since the chemical potential $\mu$ is dressed by the quasiomentum as $\mu = \mu_{\rm ntl} + (g + g_{12})/2 + k^2/2$, the deviation of the loop center from $k = 0$ must be accompanied by a tilt of loop due to the asymmetry in $k^2/2$ with respect to $k \neq 0$. The loop size can be calculated following the results in Ref. [26] and the region over which the loop extends in momentum space is given by $-k_c - \delta/(2\gamma) \leq k \leq k_c - \delta/(2\gamma)$ with $k_c = \left(|g_{12}-g|^{\frac{2}{3}} - \Omega^{\frac{2}{3}}\right)^{\frac{3}{2}}/(2\gamma)$. The edges of loop are at $\pm k_c - \delta/(2\gamma)$ and are shown by vertical dashed lines in Figs. 1(c)-(e). The size of the loops depends on the parameters $|g_{12}-g|^{\frac{2}{3}} - \Omega^{\frac{2}{3}}$ and $\gamma$. Two loops of different sizes for different values of $|g_{12}-g|$ are shown in Figs. 1(c) and (d) .

The existence of the loop structures leads to nontrivial dynamics. To show this we study nonlinear Landau-Zener transitions by applying a very weak constant acceleration force $F$ to the atoms [23, 46]. The BEC is initially prepared in the ground state of the system labeled by the lower red dot in Fig. 2(a). The constant force accelerates atoms to move along the nonlinear dispersion [indicated by an arrow in Fig. 2(a)], and once the atoms arrive at the edge of the loop [indicated by a vertical line], there is no trajectory for them to go and they have no choice but to jump to the upper or lower bands. The finite possibility for this jump to bring
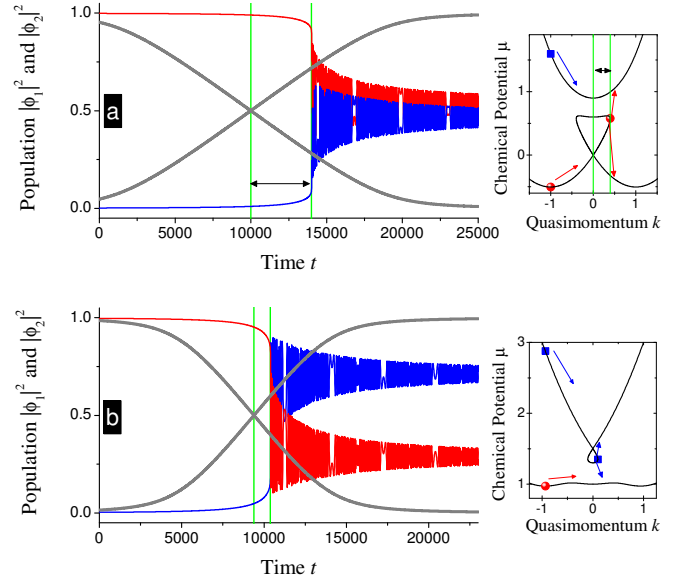


FIG. 2. Nonlinear Landau-Zener dynamics in the presence of the loop structures. The acceleration force is given by $F = 0.0001$, and the other parameters are $\Omega = 0.3, \gamma = 1$ and $\delta = 0$. The right panels show the nonlinear dispersion relations and the left panels display the dynamics for different initial states. (a): Loop in the lower band. The initial state corresponding to the thick grey lines in the left plot is prepared in the upper band (square in the right plot) and the initial state for the thin lines is in the lower band (the lower circle in the right plot). $g_{11} = g_{22} = g = 0$ and $g_{12} = 1.5$. (b): Loop in the upper band. The initial state for the thick lines in the left plot corresponds to the circle in the right plot, and that for the thin lines corresponds the square in the right plot. $g_{11} = g_{22} = g = 1.5$ and $g_{12} = 0.8$.

the atom into the upper band constitutes a nonlinear Landau-Zener transition, no matter how weak the acceleration force is. Since the nonlinear Landau-Zener transition physically originates from loop structures, it does not have a linear analogue and is a fully nonlinear effect. We stimulate the dynamics by numerical integration of Eq. (1) in momentum space, The acceleration force $F$ changes quasimomentum as $k(t) = k_{\rm ini} + Ft$ with $k_{\rm ini}$ being initial quasimomentum [47]. The time evolution of the population in $\Phi_1$ and $\Phi_2$ for different initial states is shown in Fig. 2(a), where thin lines correspond to the initial state in the lower nonlinear band and the initial state of the data shown by the thick grey lines is in the upper band [represented by a blue square].

The dynamics for these two different initial states can be seen to be quiet different. Due to finite energy gap and weak acceleration force, atoms initially in the upper band smoothly move along the upper band and change their spin-compositions. At a certain time [indicated by a vertical line], the two components become population-balanced, which in the dispersion relation corresponds to the atoms arriving at $k = 0$ in the upper band and the spin becoming unpolarized. Due to the existence of

the loop structure, the atoms in the lower band undergo nonlinear Landau-Zener tunneling. After they arrive at the loop edge, the populations show regular oscillations and one may intuitively think about the periodic motion as population oscillations between the two spin-orbit-coupled bands. As shown by thin lines in the left panel of Fig. 2(a), before the atoms arrive at the loop edge, the spin-compositions evolve smoothly, and follow the dispersion relation. Different initial states respond differently to the same acceleration force, which can be used to experimentally measure the size of loop structures. The distance between the two vertical lines in the left panel exactly corresponds to the length between $k = 0$ and the loop edge in the dispersion relation depicted in the right panel. In experiments, the time evolution of the populations can be measured in a spin-resolved Stern-Gerlach time-of-flight setup.

We also numerically check the case where the loop structures appear in the upper band. Typical results are shown in Fig. 2(b). Since the loop occurs in the upper band, atoms initial in the upper band can undergo nonlinear Landau-Zener tunneling, with the fast oscillations [thin lines in the left panel] indicating that the atoms have arrived at the loop edge in the dispersion. In this case the atoms initial in the lower band evolute smoothly. Similar to the case of loops in the lower band, one may compare the dynamics of different initial states to extract the information about the loop size.

The above dynamics of nonlinear Landau-Zener tunneling reveals that a nonlinear dispersion relation truly has a fundamental effect on nonlinear dynamics. This motivates us to study further nonlinear effects in quench dynamics, where a sudden jump of the Rabi frequency from $-\Omega$ to $\Omega$ occurs. Such a sign change can be implemented in experiments by adjusting the relevant phases between the two Raman lasers. The changing of the sign of $\Omega$ does not modify the nonlinear dispersion relation, as equation (4) has the symmetry $\mathcal{P}_\Omega \sigma_z$ with $\mathcal{P}_\Omega$ flipping the sign of $\Omega$, i.e., $\mathcal{P}_\Omega^\dagger \Omega \mathcal{P}_\Omega = -\Omega$. However, the eigenstates of systems with opposite signs of $\Omega$ are different. Such a quench technique has, for example, already been used to explore the Zitterbewegung in spin-orbit-coupled atoms [22].

To study the quench dynamics in the presence of loops, we follow the experiment procedure described in [22] and prepare ground states in the lower band [indicated by the lowest dots in the left panels of Fig. 3]. We then track the evolution of the population difference $|\Phi_1|^2 - |\Phi_2|^2$ after changing from $-\Omega$ to $\Omega$. Since it is known from experiments that the quench does not change the quasimomentum for a very long time [22], we will only use a fixed quasimomentum in the following. In the presence of loops, there are four bands for a fixed quasimomentum, which are represented by open dots in Fig. 3(a). One may intuitively expect that the dynamics following the quench would be a complicate oscillation between these
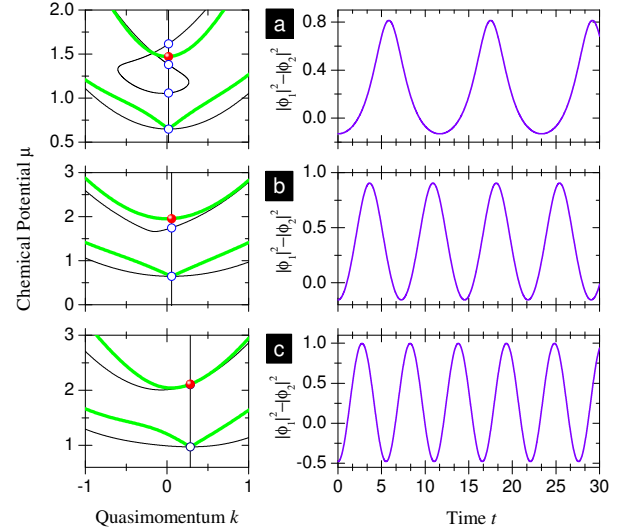


FIG. 3. (Color Online) Nonlinear dynamics induced by the quenching of the Rabi frequency from $-\Omega$ to $\Omega$ for different values of the nonlinear coefficients and $\gamma = 0.6$ and $\delta = 0.2$. In the right hand side panels, the quench dynamics is shown by the evolution of the population difference $|\Phi_1|^2 - |\Phi_2|^2$. In the left hand side panels, the nonlinear dispersion $\mu(k)$ (thin back lines) and the collective excitations $\omega(q)$ (thick green lines) are displayed together. Open circles are eigenvalues for a fixed quasimomentum, and solid circles are the excitations for a fixed quasimomentum of excitations. (a): Nonlinear dynamics in the present of a loop structure in the upper band. $\Omega = 0.4$, $g_{11} = g_{22} = g = 1.5$ and $g_{12} = 0.2$. The values of the open circles are $\mu = (1.62, 1.38, 1.06, 0.65)$ from top to bottom. The value of solid circle is $\mu = 1.47$. The oscillation period is $T = 11.67$. (b) Nonlinear dynamics in the absence of loop structure. $\Omega = 1$, $g = 1.5$ and $g_{12} = 0.8$. The open circles represent $\mu = (0.65, 1.75)$, and the location of solid circle is at $\mu = 1.95$. The oscillation period is $T = 7.26$. (c) Effective linear dynamics with the parameters $\Omega = 1$ and $g = g_{12} = 1.5$. The open and solid circles overlap, $\mu = (2.11, 0.97)$ from top to bottom. The oscillation period is $T = 5.52$, which exactly matches with the energy difference between the top and bottom circles.

four states, possessing multiple periods. However, the population difference evolution shown in the right panel of Fig. 3(a) indicates that the dynamics is periodic but with only one frequency. Furthermore, this frequency does not match up with the energy differences between any two of the four bands.

This indicates that the loops are completely irrelevant to the quench dynamics and we compare these results to a parameters region where the loops are absent and where the nonlinear dispersion has two bands for fixed quasimomentum [depicted by thin lines in the left panel of Fig. 3(b)]. The quench dynamics is again periodic [see the right panel], but its oscillation frequency still does not correspond to the energy difference between the two bands.

If one imagines the quench of the sign of $\Omega$ as a perturbation to the ground states, one can have a collective

excitation dispersion relations $\omega(q)$ with only two bands. These collective excitation bands are shown in the left panels by thick green lines. They are calculated from the Bogoliubov de Gennes equations [19, 48], and in experiments can be measured by Bragg spectroscopy [20, 21]. We have checked that the period of the quench dynamics has no relation with the energy difference between the two collective excitation bands.

The quench dynamics experiment described by Qu *et al.* in [22] surprisingly connects with the single-particle dispersion, as in their $^{87}$Rb atomic BECs, the nonlinear coefficients approximately satisfy $g_{12} = g$. According to our nonlinear two-level model in Eq. (5), one sees that their system is effectively a single-particle model, since the nonlinear term disappears when $g_{12} - g = 0$. For the case of $g_{12} - g = 0$, nonlinear dispersion is just an overall displacement of linear dispersion, which can be seen from Eq. (5) and $\mu = \mu_{\mathrm{ntl}} + (g + g_{12})/2 + k^2/2$. In Fig. 3(c), we show the nonlinear dispersion for $g_{12} = g$ and verify that the oscillation frequency of the quench dynamics in the right panel matches up with the energy difference between two circles in the left. It is very interesting to note that the oscillation frequency also equals to the difference between two collective excitation bands labeled by thick green lines.

As there is no direct relation between the quench dynamics and the nonlinear dispersion relation, the quench dynamics may be understood from a semiclassical analysis [49]. By defining $\Phi_1 = |\Phi_1|e^{i\theta_1}$, $\Phi_2 = |\Phi_2|e^{i\theta_2}$, and $n = |\Phi_2|^2 - |\Phi_1|^2$, $\theta = \theta_2 - \theta_1$, the nonlinear two-level model in Eq. (5) has a classical Hamiltonian as $H_c = (g_{12}-g)n^2/2 + 2(\gamma k + \delta/2)n - \Omega\sqrt{1-n^2}\cos(\theta)$ [26]. In the phase space of $(n, \theta)$, the oscillations induced by the quench are closed orbits around the fixed points of $H_c$, which feature one period. The oscillation frequency depends on the nonlinearity [26, 49].

In conclusion, we have investigated two kinds of nonlinear dynamics in spin-orbit-coupled BECs. For the adiabatic motions induced by a weak constant acceleration force, the atoms undergo nonlinear Landau-Zener tunneling in the presence of an interesting loop structures in the nonlinear dispersion relation. At the same time, for a quench dynamics we have found that no connection to the nonlinear dispersion relation exists.

* [yongping11@t.shu.edu.cn](yongping11@t.shu.edu.cn)

[1] Y. -J. Lin, K. Jiménez-García, and I. B. Spielman, Nature, **471**, 83 (2011). Spin-orbit-coupled Bose-Einstein condensates.

[2] N. Goldman, G. Juzeliūnas, P. Öhberg, and I. B. Spielman, Rep. Prog. Phys. **77**, 126401 (2014). Light-induced gauge fields for ultracold atoms.

[3] J. Zhang, H. Hu, and X. -J. Liu, Annual Review of Cold Atoms and Molecules **2**, 81 (2014). Fermi gases with synthetic spin-orbit coupling.

[4] H. Zhai, Rep. Prog. Phys. **78**, 026001 (2015). Degenerate quantum gases with spin-orbit coupling: a review.

[5] Y. Xu and C. Zhang, Int. J. Mod. Phys. B **29**, 1530001 (2015). Topological Fulde-Ferrell superfluids of a spin-orbit coupled Fermi gas.

[6] Y. Li, G. I. Martone, S. Stringari, Annual Review of Cold Atoms and Molecules, **3**, 201 (2015). Bose-Einstein condensation with spin-orbit coupling.

[7] S. Zhang, W. S. Cole, A. Paramekanti, and N. Trivedi, Annual Review of Cold Atoms and Molecules, **3**, 135 (2015). Spin-orbit coupling in optical lattices.

[8] Y. Zhang, M. E. Mossman, Th. Busch, P. Engels, and C. Zhang, Front. Phys. **11**, 118103 (2016). Properties of spin-orbit-coupled Bose-Einstein condensates.

[9] Z. Fu, P. Wang, S. Chai, L. Huang, and J. Zhang, Phys. Rev. A **84**, 043609 (2011). Bose-Einstein condensate in a light-induced vector gauge potential using 1064-nm optical-dipole-trap lasers.

[10] C. Wang, C. Gao, C. -M. Jian, and H. Zhai, Phys. Rev. Lett. **105**, 160403 (2010). Spin-orbit coupled spinor Bose-Einstein condensates.

[11] T. -L. Ho and S. Zhang, Phys. Rev. Lett. **107**, 150403 (2011). Bose-Einstein condensates with spin-orbit interaction.

[12] C. -J. Wu, I. Mondragon-Shem, and X. -F. Zhou, Chin. Phys. Lett. **28**, 097102 (2011). Unconventional Bose-Einstein condensations from spin-orbit coupling.

[13] S. Sinha, R. Nath, and L. Santos, Phys. Rev. Lett. **107**, 270401 (2011). Trapped two-dimensional condensates with synthetic spin-orbit coupling.

[14] H. Hu, B. Ramachandhran, H. Pu, and X. -J. Liu, Phys. Rev. Lett. **108**, 010402 (2012). Spin-orbit coupled weakly interacting Bose-Einstein condensates in harmonic traps.

[15] Y. Li, L. P. Pitaevskii, and S. Stringari, Phys. Rev. Lett. **108**, 225301(2012). Quantum tricriticality and phase transitions in spin-orbit coupled Bose-Einstein condensates.

[16] Y. Li, G. I. Martone, L. P. Pitaevskii, and S. Stringari, Phys. Rev. Lett. **110**, 235302 (2013). Superstripes and the excitation spectrum of a spin-orbit-coupled Bose-Einstein condensate.

[17] C. Hamner, C. Qu, Y. Zhang, J. Chang, M. Gong, C. Zhang, and P. Engels, Nat. Commun. **5**, 4023 ( 2014). Dicke-type phase transition in a spin-orbit-coupled Bose-Einstein condensate.

[18] J. -Y. Zhang, S. -C. Ji, Z. Chen, L. Zhang, Z. -D. Du, B. Yan, G. -S. Pan, B. Zhao, Y. -J. Deng, H. Zhai, S. Chen, and J. -W. Pan, Phys. Rev. Lett. **109**, 115301 (2012). Collective dipole oscillations of a spin-orbit coupled Bose-Einstein condensate.

[19] W. Zheng, Z. -Q. Yu, X. Cui, and H. Zhai, J. Phys. B:

At. Mol. Opt. Phys. **46** 134007 (2013). Properties of Bose gases with the Raman-induced spin-orbit coupling.

[20] M. A. Khamehchi, Y. Zhang, C. Hamner, Th. Busch, and P. Engels, Phys. Rev. A **90**, 063624 (2014). Measurement of collective excitations in a spin-orbit-coupled Bose-Einstein condensate.

[21] S. -C. Ji, L. Zhang, X. -T. Xu, Z. Wu, Y. Deng, S. Chen, and J. -W. Pan, Phys. Rev. Lett. **114**, 105301 (2015). Softening of roton and phonon modes in a Bose-Einstein condensate with spin-orbit coupling.

[22] C. Qu, C. Hamner, M. Gong, C. Zhang, and P. Engels, Phys. Rev. A **88**, 021604(R) (2013). Observation of Zitterbewegung in a spin-orbit-coupled Bose-Einstein condensate.

[23] A. J. Olson, S. -J. Wang, R. J. Niffenegger, C. -H. Li, C. H. Greene, and Y. P. Chen, Phys. Rev. A **90**, 013616 (2014). Tunable Landau-Zener transitions in a spin-orbit-coupled Bose-Einstein condensate.

[24] J. -R. Li, J. Lee, W. Huang, S. Burchesky, B. Shteynas, F. Ç. Top, A. O. Jamison, and W. Ketterle, Nature **543**, 91 (2017). A stripe phase with supersolid properties in spin-orbit-coupled Bose-Einstein condensates.

[25] B. Wu and Q. Niu, Phys. Rev. A **61**, 023402 (2000). Nonlinear Landau-Zener tunneling.

[26] J. Liu, L. Fu, B. -Y. Ou, S. -G. Chen, D. -II Choi, B. Wu, and Q. Niu, Phys. Rev. A **66**, 023404 (2002). Theory of nonlinear Landau-Zener tunneling.

[27] Y.-A. Chen, S. D. Huber, S. Trotzky, I. Bloch, and E. Altman, Nat. Phys. **7**, 61 (2011). Many-body Landau-Zener dynamics in coupled one-dimensional Bose liquids.

[28] K. Jiménez-García, L. J. LeBlanc, R. A. Williams, M. C. Beeler, C. Qu, M. Gong, C. Zhang, and I. B. Spielman, Phys. Rev. Lett. **114**, 125301 (2015). Tunable spin-orbitc oupling via strong driving in ultracold-atom systems.

[29] Y. Zhang, G. Chen, and C. Zhang, Sci. Rep. **3**, 1937 (2013). Tunable spin-orbit coupling and quantum phase transition in a trapped Bose-Einstein condensate.

[30] B. Wu, R. B. Diener, and Q. Niu, Phys. Rev. A **65**, 025601 (2002). Bloch waves and bloch bands of Bose-Einstein condensates in optical lattices.

[31] D. Diakonov, L. M. Jensen, C. J. Pethick, and H. Smith, Phys. Rev. A **66**, 013604 (2002). Loop structure of the lowest Bloch band for a Bose-Einstein condensate.

[32] E. J. Mueller, Phys. Rev. A **66**, 063603 (2002). Superfluidity and mean-field energy loops: hysteretic behavior in Bose-Einstein condensates.

[33] M. Machholm, C. J. Pethick, and H. Smith, Phys. Rev. A **67**, 053613 (2003). Band structure, elementary excitations, and stability of a Bose-Einstein condensate in a periodic potential.

[34] B. T. Seaman, L. D. Carr, and M. J. Holland, Phys. Rev. A **72**, 033602 (2005). Period doubling, two-color lattices, and the growth of swallowtails in Bose-Einstein condensates.

[35] I. Danshita and S. Tsuchiya, Phys. Rev. A **75**, 033612 (2007). Stability of Bose-Einstein condensates in a Kronig-Penney potential.

[36] Y. Lin, R.-K. Lee, Y.-M. Kao, and T.-F. Jiang, Phys. Rev. A **78**, 023629 (2008). Band structures of a dipolar Bose-Einstein condensate in one-dimensional lattices.

[37] S. B. Koller, E. A. Goldschmidt, R. C. Brown, R. Wyllie, R. M. Wilson, and J. V. Porto, Phys. Rev. A **94**, 063634 (2016). Nonlinear looped band structure of Bose-Einstein condensates in an optical lattice.

[38] B. Prasanna Venkatesh, J. Larson, and D. H. J. O'Dell, Phys. Rev. A **83**, 063606 (2011). Band-structure loops and multistability in cavity QED.

[39] L. Dong, L. Zhou, B. Wu, B. Ramachandhran, and H. Pu, Phys. Rev. A **89**, 011602(R) (2014). Cavity-assisted dynamical spin-orbit coupling in cold atoms.

[40] K. Porsezian, and K. Senthilnathan, Chaos **15**, 037109 (2005). Generation of Bragg solitons through modulation instability in a Bragg grating structure.

[41] Z. Chen and B. Wu, Phys. Rev. Lett. **107**, 065301 (2011). Bose-Einstein condensate in a honeycomb optical lattice: fingerprint of superfluidity at the Dirac point.

[42] R. W. Bomantara, W. Zhao, L. Zhou, and J. Gong, Phys. Rev. B **96**, 121406(R) (2017). Nonlinear Dirac cones.

[43] I. Yu. Chestnov, A. V. Yulin, A. P. Alodjants, and O. A. Egorov, Phys. Rev. B **94**, 094306 (2016). Nonlinear Bloch waves and current states of exciton-polariton condensates.

[44] G. Watanabe, S. Yoon, and F. Dalfovo, Phys. Rev. Lett. **107**, 270404 (2011). Swallowtail band structure of the superfluid Fermi gas in an optical lattice.

[45] D. Yu, W. Yi, and W. Zhang, Phys. Rev. A **92**, 033623 (2015). Swallowtail structure in Fermi superfluids with periodically modulated interactions.

[46] J. M. Gomez Llorente and J. Plata, Phys. Rev. A **94**, 053605 (2016). Acceleration of spin-orbit-coupled Bose-Einstein condensates: Analytical description of the emergence of Landau-Zener transitions.

[47] N. W. Aschcoft and N. D. Mermin, Solid State Phsyics (Saunders College, Philadelphia, 1976).

[48] G. I. Martone, Y. Li, L. P. Pitaevskii, and S. Stringari, Phys. Rev. A **86**, 063621 (2012). Anisotropic dynamics of a spin-orbit-coupled Bose-Einstein condensate.

[49] A. Smerzi, S. Fantoni, S. Giovanazzi, and S. R. Shenoy, Phys. Rev. Lett. **79**, 4950 (1997). Quantum coherent atomic tunneling between two trapped Bose-Einstein condensates.